



HAL
open science

Crossing of the Branch Cut: The Topological Origin of a Universal 2π -Phase Retardation in Non-Hermitian Metasurfaces

Rémi Colom, Elena Mikheeva, Karim Achouri, Jesus Zuniga-perez, Nicolas Bonod, Olivier J F Martin, Sven Burger, Patrice Genevet

► To cite this version:

Rémi Colom, Elena Mikheeva, Karim Achouri, Jesus Zuniga-perez, Nicolas Bonod, et al.. Crossing of the Branch Cut: The Topological Origin of a Universal 2π -Phase Retardation in Non-Hermitian Metasurfaces. *Laser and Photonics Reviews*, 2023, 17 (6), 10.1002/lpor.202200976 . hal-04308666

HAL Id: hal-04308666

<https://cnrs.hal.science/hal-04308666>

Submitted on 27 Nov 2023

HAL is a multi-disciplinary open access archive for the deposit and dissemination of scientific research documents, whether they are published or not. The documents may come from teaching and research institutions in France or abroad, or from public or private research centers.

L'archive ouverte pluridisciplinaire **HAL**, est destinée au dépôt et à la diffusion de documents scientifiques de niveau recherche, publiés ou non, émanant des établissements d'enseignement et de recherche français ou étrangers, des laboratoires publics ou privés.

Crossing of the Branch Cut: The Topological Origin of a Universal 2π -Phase Retardation in Non-Hermitian Metasurfaces

Rémi Colom,* Elena Mikheeva, Karim Achouri, Jesus Zuniga-Perez, Nicolas Bonod, Olivier J. F. Martin, Sven Burger, and Patrice Genevet*

Full wavefront control by photonic components requires that the spatial phase modulation on an incoming optical beam ranges from 0 to 2π . Because of their radiative coupling to the environment, all optical components are intrinsically non-Hermitian systems, often described by reflection and transmission matrices with complex eigenfrequencies. Here, it is shown that parity or time symmetry breaking—either explicit or spontaneous—moves the position of zero singularities of the reflection or transmission matrices from the real axis to the upper part of the complex frequency plane. A universal 0 to 2π -phase gradient of an output channel as a function of the real frequency excitation is thus realized whenever the discontinuity branch bridging a zero and a pole, that is, a pair of singularities, is crossing the real axis. This basic understanding is applied to engineer electromagnetic fields at interfaces, including, but not limited to, metasurfaces. Non-Hermitian topological features associated with exceptional degeneracies or branch cut crossing are shown to play a surprisingly pivotal role in the design of resonant photonic systems.

design. A particularly impressive amount of research in the field of metamaterials has been devoted to the design and realization of ultra-thin artificial optical surfaces for wavefront engineering and control. These optical surfaces, also dubbed metasurfaces, rely on the coherent scattering of light by a sizable distribution of nanoscatterers of various shapes and material compositions. The list of optical effects achieved using metasurfaces is extensive, ranging from anomalous reflection and refraction,^[1–8] all the way to the design of utterly complex vectorial holographic surfaces.^[9–15] In practice, light control is achieved by varying the geometries of adjacent elements so as to provide spatially-varying phase retardation on the incoming wavefront. The realization of ultrathin optical components capable of arbitrarily shaping the

wavefront of a light beam to create metalenses, metadeflectors, metaholograms, metasurfaces generating optical vortices, and so on^[16–19], requires full 2π phase modulation. It is thus necessary to identify which are the leading physical mechanisms of interest to achieve full 2π phase delay at nanoscale for a desired reflection or transmission channel. The physical mechanisms of

1. Introduction

Over the last decades, the development of artificial materials and artificial interfaces to address arbitrarily output-from-input signals has considerably modernized the fields of optics and optical

R. Colom, S. Burger
Zuse Institute Berlin
Takustraße 7, 14195 Berlin, Germany
E-mail: remi.colom@crhea.cnrs.fr


R. Colom, E. Mikheeva, J. Zuniga-Perez, P. Genevet
Université Côte d'Azur
CNRS
CRHEA
Valbonne 06560, France
E-mail: patrice.genevet@crhea.cnrs.fr

K. Achouri, O. J. F. Martin
Ecole Polytechnique Federale de Lausanne
Lausanne, VD Switzerland

J. Zuniga-Perez
MajuLab
International Research Laboratory IRL 3654, CNRS
Université Côte d'Azur
Sorbonne Université
National University of Singapore
Nanyang Technological University
Singapore Singapore

N. Bonod
Aix-Marseille Univ
CNRS
Centrale Marseille
Institut Fresnel
Marseille 13397, France

S. Burger
JCMwave GmbH
Bolivarallee 22, 14050 Berlin, Germany

 The ORCID identification number(s) for the author(s) of this article can be found under <https://doi.org/10.1002/lpor.202200976>

© 2023 The Authors. Laser & Photonics Reviews published by Wiley-VCH GmbH. This is an open access article under the terms of the Creative Commons Attribution License, which permits use, distribution and reproduction in any medium, provided the original work is properly cited.

DOI: 10.1002/lpor.202200976

interest for the design of these phase building blocks include the Pancharatnam–Berry phase in anisotropic nanoparticles,^[20,21] effective index waveguide modes in nanopillars,^[2] and the 2π -phase modulation associated with resonant scattering of Mie nanoparticles or plasmonic metasurface. Yet not all resonant metasurfaces can provide a modulation spanning the whole 2π range with many metasurfaces providing only a π phase accumulation. Therefore, there is a need for a general condition which would simplify the identification of metasurfaces spanning the full 2π range. Ultimately, and despite all the efforts in understanding which physical mechanisms are leading to optimal designs, the most advanced patterns often require witless numerical parameter searches.

Here, we identify the link between the full 2π -phase retardation commonly used for designing metasurfaces and the relative spectral positions of topological singularities of the metasurface response functions. These topological singularities manifest as zero-pole pairs in the complex-frequency plane. Relying on the work realized in refs. [22, 23] in the framework of the \mathbf{S} -matrix, we report on a sufficient condition on the relative positions of these zero-pole pairs on selected reflection or transmission channels to achieve the whole $[0, 2\pi]$ phase gradient needed for wavefront shaping metasurfaces working either in reflection or in transmission. We also exploit these insights to explain the physical mechanism behind existing phase-gradient resonant metasurface designs, in particular the dielectric Huygens metasurfaces.^[24] Resonant-phase metasurfaces are designed to connect N input \mathbf{E}_{in} -modes with N output \mathbf{E}_{out} -modes. They behave as regular linear open wave systems mathematically described by $N \times N$ response matrices $\mathbf{F}(\omega)$ such that, $\mathbf{E}_{\text{out}} = \mathbf{F}(\omega) \cdot \mathbf{E}_{\text{in}}$,^[25,26] where $\mathbf{F}(\omega)$ represents either the \mathbf{S} -matrix, the reflection matrix \mathbf{R} or the transmission matrix \mathbf{T} .^[27] In the context of diffraction gratings, analysis based on zeros and poles of the \mathbf{S} -matrix coefficients was used to determine the origin of such phenomena as Wood's anomalies or total absorption of light.^[28–31] Zeros and poles of response matrices or functions behave as phase singularities around which the phase is spiraling in a vortex-like way.^[22,23] Metasurfaces, like most optical devices, are intrinsically non-Hermitian devices, suffering from scattering losses and potentially from intrinsic loss or gain. Therefore, their phase singularities generally occur in the complex frequency plane. Singularities have long been known to play an important role in optics.^[32–35] Here, we show how phase singularities occurring in the complex plane greatly influence the optical response of resonant metasurfaces. More precisely, we show that 2π phase accumulation needed for wavefront engineering of reflected or transmitted output channel has a deep topological origin. It requires two complementary singularities, known as poles and zeros, to be disposed in the complex frequency plane on either side of the real axis. This way, the branch-cut discontinuity bridging these two singularities crosses the real axis, providing 2π phase accumulation as a function of the real frequency excitation. Note that this result has important implications for the design of metasurfaces since structures displaying a 2π phase accumulation as a function of the frequency is often used as a starting point to realize phase-gradient metasurfaces. We demonstrate that one can rely on symmetry-breaking in order to have two singularities of the same pair located on each side of the real axis which induces 2π circulation for any path in the complex plane encircling a sin-

gularity. We propose two approaches inducing parity or time symmetry breaking to move the zeros from the real axis to the upper part of the complex plane.

The first solution relies on symmetry breaking arguments. We show that breaking parity-time symmetry by using, for example, symmetry breaking in the z -direction (i.e., perpendicular to the metasurface plane) provides an additional degree of freedom for designing phase-gradient metasurfaces working in reflection. This method empowers metasurface's designers with a new approach for phase-gradient metasurfaces.

The second solution, which is linked to the regime known as Huygens metasurfaces,^[24] is more subtle as it occurs in symmetric systems featuring spontaneously symmetry-broken states. We thus show that the physical origin of Huygens metasurfaces is deeply rooted in topological concepts. Finally, looking at the analytical expressions of metasurface boundary conditions, namely the “generalized sheet transition conditions” (GSTC), we identified the symmetry conditions of the electromagnetic modes to be considered for spontaneous symmetry-breaking.

2. Complex Frequency Analysis and Phase Integration

We begin our analysis by studying the analytical properties of a non-Hermitian metasurface represented by a response function $F(\omega)$, for example, its reflection R or its transmission T coefficients. If we assume that $F(\omega)$ only possesses simple zeros and poles, it can be expanded using Weierstrass theorem leading to the following expression^[22,23]

$$F(\omega) = A \exp(iB\omega) \prod_{n=-\infty}^{\infty} \frac{\omega - \omega_{z,n}}{\omega - \omega_{p,n}} \quad (1)$$

where A and B are constants depending on the properties of the metasurface and the considered response function. Similar expansions were also derived in refs. [36–38] in different contexts. By definition, the phase is given by $\text{Arg}(F) = \text{Im}(\log(F))$ and, as a consequence, zeros and poles of F correspond to logarithmic branch points at which the phase becomes singular.^[39] We refer to these zeros and poles as singularities throughout this article. The phase is thus spiraling as vortices around zeros and poles of F in the same way as the phase of a complex number in \mathbb{C} rotates around the origin of the complex plane.^[22] Zeros and poles are thus analogous to topological defects.^[40] While the poles of \mathbf{S} , R , and T are identical and are associated with resonances or quasi-normal modes solutions of the wave equation, their complex zeros are different and provide insights into the physical effects governing the metasurface response. In particular, they greatly influence the real-frequency response of metasurfaces. Zeros of the \mathbf{S} -matrix are complex conjugate of poles for passive lossless metasurfaces and can reach the real axis in lossy structures, where they are linked to perfect coherent absorption.^[23,41,42] Zeros of R and T coefficients are linked to reflectionless and transmissionless states, respectively.^[25,26,43] Let us consider a toy-model $F(\omega) = (\omega - \omega_z)/(\omega - \omega_p)$, derived from Equation (1) for $A = 1$ and $B = 0$ and considering a single zero–pole pair, featuring only one zero ω_z and one pole ω_p located on each side of the real axis, as indicated by the blue and red regions respectively in **Figure 1a**.

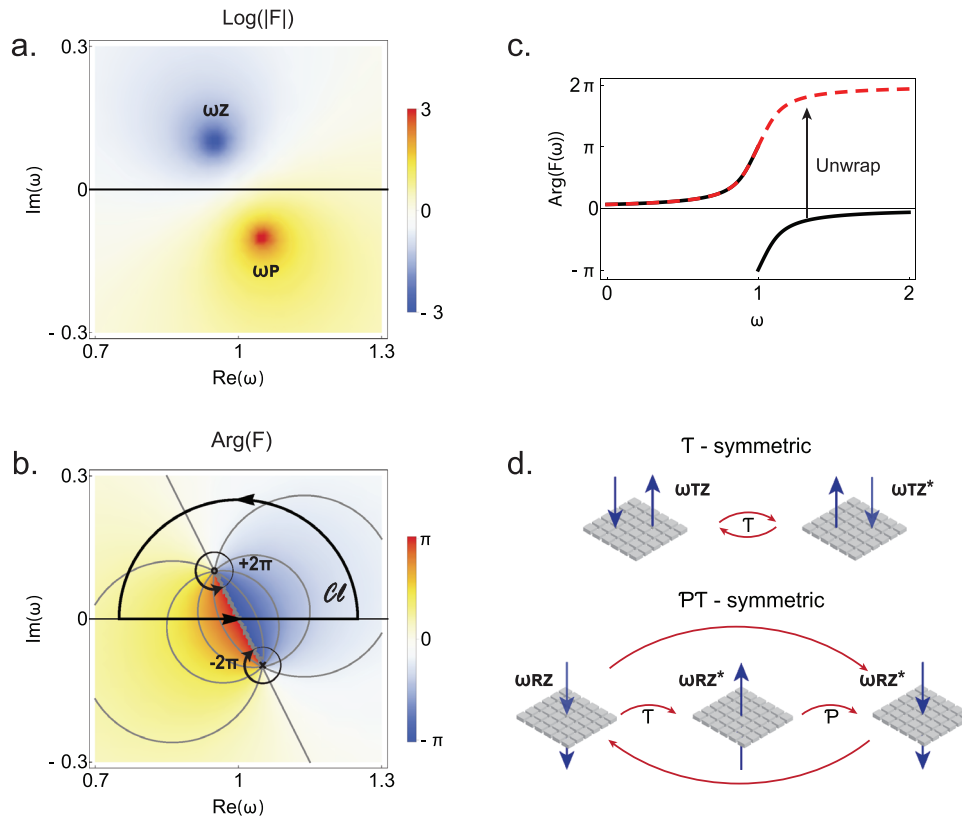


Figure 1. Illustration of 2π -phase accumulation concept relying on symmetry-breaking to position zero and pole across the real axis. a) Logarithmic map of a simplified model of metasurface optical response $F(\omega) = (\omega - \omega_z)/(\omega - \omega_p)$ as a function of the real and imaginary parts of the complex frequency, with ω_z and ω_p , chosen so as to be in the upper part, and respectively in the lower part, of the complex plane. b) Argument of $F(\omega)$ in (a) as a function of the real and imaginary part of the complex frequency featuring phase singularities at the positions of the zero and the pole of $F(\omega)$. Overlay black contour C_1 encircling the zero used for the complex plane integration. c) Wrapped and unwrapped phase of $F(\omega)$ as a function of the (real) frequency. The discontinuity at $\omega = 1$ results from crossing the branch cut observed in (b). d) Schematics of metasurfaces operating in reflection and respectively in transmission, supporting time-reversal (T) transmissionless state at frequency ω_{TZ} and respectively parity-time (PT) reflectionless state at frequency ω_{RZ} .

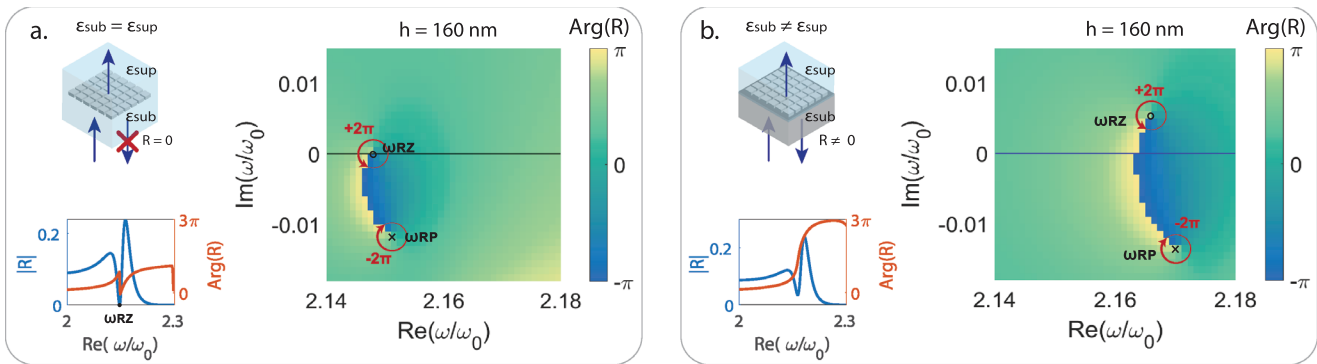
We define as topological charge the quantity q calculated by evaluating the winding number along a counterclockwise contour encircling the singularities as [40, 44]

$$q = \frac{1}{2\pi} \oint_{C_1} \frac{d\text{Arg}(F(\omega))}{d\omega} d\omega \quad (2)$$

equaling to $q = +1$ for a zero and $q = -1$ for a pole (see Supporting Information). The phase varies by 2π around the zeros and the poles with an opposite sign. As a result, the phase variation around both is null, see Figure 1b. Moreover, zeros and poles occur in pairs and are connected by a phase discontinuity, also called branch cut. This can be seen in the panel in Figure 1b for a single zero–pole pair. In our example, the complex zero and pole values are purposely chosen such that the branch cut is crossing the real axis. The sufficient condition for a metasurface to support a 2π resonant phase accumulation as a function of the real frequency is thus to possess a zero–pole pair separated by the real axis, as illustrated in Figure 1c. After unwrapping the phase discontinuity resulting from crossing the branch cut at $\omega = 1$, we obtain a 2π phase difference $\Delta\text{Arg}(F) = \text{Arg}(F(\omega_2)) - \text{Arg}(F(\omega_1))$ as $\omega_1 \rightarrow 0$ and $\omega_2 \rightarrow 2$ (see

Figure 1c). This link between existence of a zero–pole pair separated by the real axis and a phase accumulation of 2π on the real axis was also evidenced in refs. [22, 23] for the S -matrix coefficients. This behavior becomes extremely relevant for wavefront engineering when it occurs, as shown herein, for R and T -matrix coefficients, simply because these are responsible for wavefront modulation in reflection and transmission, respectively. It may be further understood by using Cauchy's residue theorem. To show this, let us compute $\Delta\text{Arg}(F) = \int_{\omega_1}^{\omega_2} \frac{d\text{Arg}(F(\omega))}{d\omega} d\omega$ by first considering the integral of $d\text{Arg}(F(\omega))/d\omega$ along a contour C_1 containing one singularity of charge q such as the one displayed in Figure 1b. It consists of the line segment $[\omega_1, \omega_2]$ closed by a semi-circle C_{sc} of radius R in the upper part of the complex plane. As a consequence, $\Delta\text{Arg}(F) = 2\pi q - \int_{C_{sc}} \frac{d\text{Arg}(F(\omega))}{d\omega} d\omega$. However, it can be shown that $\int_{C_{sc}} \frac{d\text{Arg}(F(\omega))}{d\omega} d\omega \rightarrow 0$ when the radius R increases, see Supporting Information for the exact case of the transmission coefficient. This highlights the link between the 2π phase accumulation on the real axis and existence of a zero above the real axis. The range over which the 2π phase accumulation depends on the decrease of the integral along the C_{sc} contour. Fortunately, in practice, this integral vanishes fast enough so that the

PT - symmetry breaking



Spontaneous T - symmetry breaking

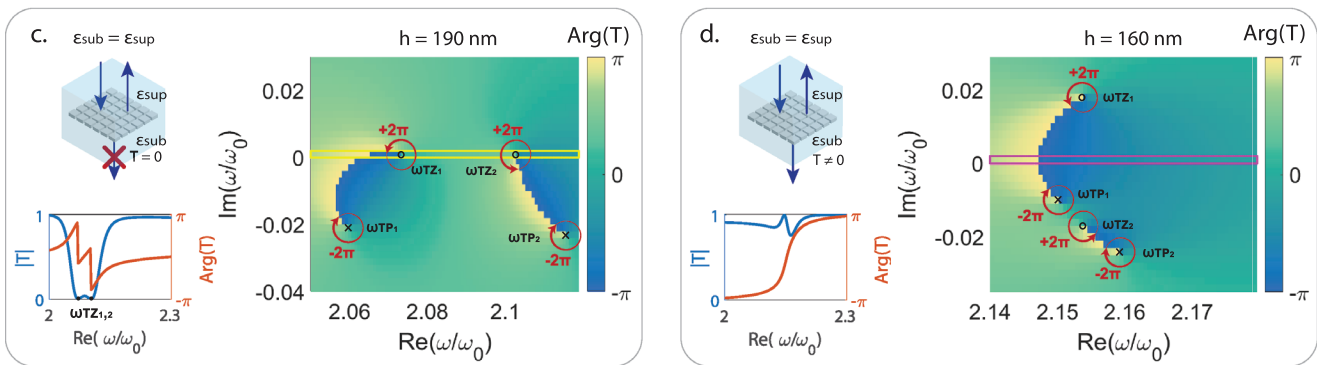


Figure 2. Examples of two types of symmetry-breaking inducing a topological singularity to cross the real axis. Each panel displays the $\text{Arg}(F)$ as a function of complex frequency ω , computed by using numerical simulations, insets show the behavior for real frequency and a schematics of the setup. a,b) Explicit P -symmetry breaking. Parity-time symmetry is preserved by surrounding the metasurface with homogeneous material. The zero sits on the real axis and the accumulated phase is smaller than 2π (a). Breaking parity symmetry is realized by modifying the refractive index of the superstrate ($\epsilon_{\text{sup}} = 2.12$) which results in displacing the zero to the upper part of the complex plane, leading to more than 2π phase accumulation in reflection (b). c,d) Spontaneous T -symmetry breaking. Two transmissionless states are present on the real axis. As a result, the transmission is modulated from 0 to 1, and poor phase coverage is achieved (c). The system is then driven to the condition known as Huygens metasurfaces by changing the height h of the building blocks from $h = 190$ nm in (c) to $h = 160$ nm in (d). One of the zeros of the two pairs is expelled in the upper complex plane. As a result, the transmission reaches almost unity and the phase accumulates up to 2π . Spontaneous symmetry breaking happens after the coalescence of zeros at EP. This process is explained in detail in Figure 3. Note that (d) structural parameters are strictly identical as in (a), indicating that the high transmission window of HMS results from the existence of an associated reflection zero ω_{RZ} . The yellow and pink rectangles in (c) and (d) are indicating the respective regions denoted by the yellow and pink rectangles in Figure 3a,b.

complete phase accumulation occurs on reasonable frequency ranges. This will be illustrated by two examples shown in Figure 2 where 2π phase accumulation occurs over moderate frequency ranges.

To conclude, the derivations carried out in this section highlight the topological character of the phase response of metasurfaces. In particular, we have shown that the phase accumulation over sufficiently large frequency ranges is quantized and only takes values of $2\pi \cdot q$ where q is the winding number defined by Equation (2) and is an integer number. We showed that q is actually counting the number of zero-pole pairs separated by the real axis (assuming they are all first order phase singularities). Importantly this disputes the common claim that metasurfaces supporting an isolated resonance provide a π phase variation. The origin of this discrepancy is linked to the behavior of the phase when a zero is on the real axis leading to a singular behavior of the phase associated with a π jump.

3. The Link between Symmetries and Positions of Zero-Point Singularities in the Complex Plane

As a consequence of causality, poles are always restricted to the lower part of the complex plane in passive systems^[36] (the convention used for the time dependence throughout this article is $e^{-i\omega t}$). It is known that in active systems, adding gain can in principle move poles upward, fulfilling thereby the lasing condition when they reach the real axis, but this is not a simple and technologically relevant solution for metasurfaces. This is, therefore, outside of the scope of the present study. A question then arises: how to design a passive structure that can support a phase singularity in the upper part of the complex plane thus displaying a 2π resonant phase accumulation over the real axis? Discarding active systems with complex pole manipulation, we propose to move zeros to the upper part of the complex plane for the reflection or the transmission coefficients. As already mentioned,

it was shown in refs. [22, 23] that for lossless structures or at least for structures featuring a small amount of loss, the zero-pole pairs of the S -matrix coefficients are usually separated by the real axis. In this case, the S -matrix coefficients display a 2π phase accumulation for each of its zero-pole pairs. In a general case of incoming and outgoing channels on both sides of the metasurface, purely incoming and outgoing fields on both sides have to be generated for observing this effect, which is not practical for the design of metasurfaces. However, when a mirror is added on one side, it is possible to engineer the phase in reflection by controlling the position of the reflection zero corresponding to total absorption in the complex plane. To our knowledge, this was first pointed out previously for a metallic grating.^[45] The behavior of the phase at the vicinity of the total-absorption condition has actually been exploited in several designs of phase-gradient metasurfaces.^[46–49] More precisely, it has been established that such metasurfaces possess different modes of operation depending on the relative values of radiative and absorption losses:^[50] i) when the absorption losses exceed radiative losses, the so-called overdamped regime, the zero of reflection is located below the real axis which prevents a full 2π phase accumulation; ii) when radiative losses are equal to absorption losses, defined as the critical coupling regime, the reflection zero is on the real axis causing a π phase discontinuity. Finally, when the radiative losses exceed the absorption losses, the underdamped regime, and the reflection zero is above the real axis which leads to a 2π phase accumulation. In the remaining of this article, we will however focus on ways to move transmission and reflection zeros to the upper half of the complex plane when there exists incoming and outgoing channels on both sides of the metasurface. To this end, one first needs to better understand the constraints imposed on the locations of the zeros in the complex plane by the symmetries of the metasurface.

3.1. Transmissionless States of a System Supporting Time-Reversal Symmetry

Any dielectric metasurface made of lossless material defines a system which is unitary. A transmissionless state characterized by a zero on the real axis in the complex frequency plane of the transmission coefficient thus imposes unity reflection at this frequency. As explained in refs. [25, 26] applying the time-reversal operator results in the complex conjugation of the frequency, the permittivities as well as the fields, thereby interchanging incoming and outgoing waves. Considering a metasurface invariant under the action of the time-reversal operator and possessing a transmission zero ω_{TZ} , time-reversal symmetry thus imposes that the metasurface also possesses a complex-conjugated transmission zero at ω_{TZ}^* . The reason why there is a complex conjugation of frequency is a consequence of time reversal along with the fact that the time-dependent fields considered are real valued (for a detailed derivation see refs. [23, 36]). Similarly, for reflectionless states, time-reversal symmetry implies that a metasurface possessing a reflection zero at ω_{RZ} , should support a reflection zero at the frequency ω_{RZ}^* for light impinging from the other side of the metasurface. This is a consequence of interchanging incoming waves with outgoing waves by the time-reversal operator.

3.2. Reflectionless States of a System Supporting Parity-Time Symmetry

The study of the underlying symmetry properties of reflectionless states necessitates considering inversion symmetry in the propagation direction (z) in addition to time-reversal symmetry.^[25] To understand these symmetry arguments, let us consider a metasurface possessing a reflection zero for light impinging from one given side at a possibly complex-valued frequency ω_{RZ} . If the metasurface is invariant under time-reversal, then it also possesses a reflection zero at ω_{RZ}^* for light impinging on the other side as illustrated in Figure 1d. In addition, the metasurface may remain invariant under the symmetry transformation which consists of an inversion with respect to its median plane. Here we consider the terminology “parity symmetry” to describe the inversion with respect to the propagation direction (z) that transforms (x, y, z) into $(x, y, -z)$. For the latter condition to be fulfilled, not only should the permittivity of the substrate ϵ_{sub} be equal to the permittivity of the top medium ϵ_{sup} but the scatterers composing the metasurface should all remain invariant under this inversion transformation as well (which is the case for the nanocubes considered in the article). A metasurface invariant under time reversal and inversion symmetry (equivalent to parity symmetry) possesses a reflection zero at both frequencies ω_{RZ} and ω_{RZ}^* for light impinging from the same side as shown Figure 1d.

3.3. Real versus Complex-Conjugate Zeros of Symmetry-Preserving Systems

These two previous paragraphs and the symmetry considerations discussed for each case indicate that the time-reversed counterpart of a transmissionless state is also a transmissionless state, and similarly, the parity-time symmetric of a reflectionless state is also a reflectionless state, as illustrated in Figure 1d. Upon conservation of symmetries, transmission or respectively reflection zeros should thus occur either at real frequencies (ω_{TZ} is real) or as conjugated pairs in the complex plane (i.e., ω_{TZ} and its complex-conjugated counterpart are located symmetrically with respect to the real axis). The former case is generic and could happen even for a single zero–pole pair, but to understand the latter case it is necessary to remind that Equation (1) associates one zero to only one pole. Therefore, symmetry-preserving systems having conjugated zeros positioned symmetrically with respect to the real axis imply necessarily the interaction of at least two zero–pole pairs.

4. Explicit or Spontaneous Symmetry-Breaking Leading to 2π -Phase Accumulation on the Real Axis

Given these symmetry constraints, two approaches can be considered to expel zeros to the upper part of the complex plane: i) Explicit breaking of a relevant symmetry, which relaxes the real-value constraint for an isolated zero, thus allowing to move it into the complex plane. This solution works both in reflection (by breaking the P or T -symmetry) and in transmission (by breaking the T -symmetry) respectively. Reflection zeros can be moved to the upper part of the complex plane by breaking the reflection

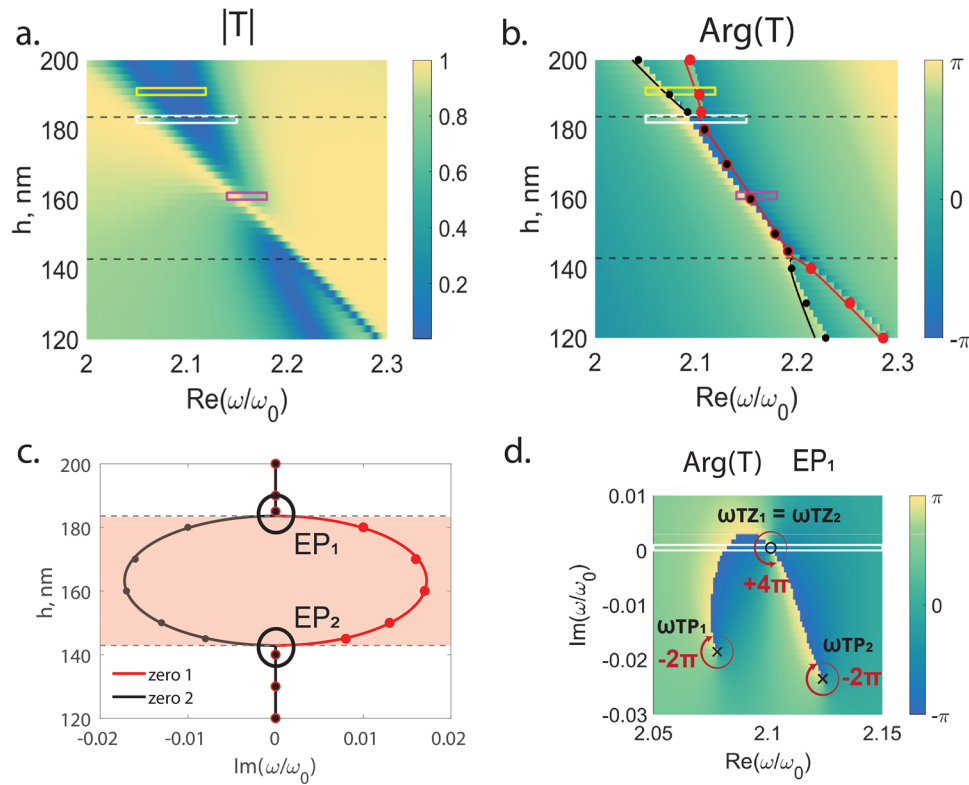


Figure 3. Huygens metasurfaces: A spontaneous T -symmetry breaking condition. a) Typical transmission spectra of metasurface operating in the Huygens regime as a function of the nanocube height h and real part of the frequency. Two transmissionless states are present in the top and bottom part of the graph, denoted by the dashed black lines. In the middle, a high transmission window opens, with near-unity transmission region indicated by the pink rectangle. b) Phase map associated to the transmission map in (a). Superposed are shown the real parts of the frequencies of the transmissionless states. They merge in two points, at the boundary of the Huygens regime, and remain with the same real frequency in-between. c) Imaginary parts of the zeros as a function of the nanocube height h . At the boundary of the Huygens regime, the imaginary part of the zero frequencies bifurcates and symmetrically moves respectively to the upper and lower parts of the complex plane as a consequence of spontaneous symmetry breaking. d) Phase map as a function of the real and imaginary part of the frequency at the coalescence of zeros $h_{EP_1} = 183.58$ nm, or EP. At the EP, the circulation of the phase is equal to 4π . The white rectangle denotes the region highlighted by the white rectangle in (a,b).

symmetry along z or loss engineering. Transmission zeros require instead the presence of gain to be moved to the upper part of the complex plane. ii) Spontaneous symmetry breaking: it was predicted in the previous section that transmission and reflection zeros of T - and PT -symmetric systems respectively, apart from being on the real axis, could exist in complex conjugated pairs. This configuration would result in the existence of a zero in the upper part of the complex plane and thus lead to a 2π phase accumulation over the real axis. This case is of a particular interest since it is a manifestation of spontaneous symmetry breaking. Let us illustrate this point for transmissionless states. These states can formally be considered to be the solutions of an eigenvalue problem corresponding to Maxwell's equations with the appropriate boundary conditions. When considering lossless (and passive) materials, this problem possesses time-reversal symmetry since both Maxwell's equations and the boundary conditions of transmissionless states are invariant under time-reversal transformation. When transmissionless states occur at real frequencies, they are also left invariant by time-reversal symmetry. However, when two transmissionless states are associated with complex-conjugated frequencies, neither of these states is left invariant by time-reversal transformation. In this configuration,

these two transmissionless states break time-reversal symmetry while the global system preserves it due to the complex conjugation. This is, in fact, a spontaneous symmetry breaking of states. This spontaneous symmetry breaking occurs at an exceptional point (EP) where two transmission zeros become degenerated. EPs thus induce a transition between real-valued transmission zeros and pairs of complex-conjugated transmission zeros. In Section 5, we will show that the transmission properties of dielectric Huygens metasurfaces are in fact consequences of this phenomenon. This is illustrated in **Figure 3** and in the videos provided in Supporting Information. These results confirm that in the region where transmission zeros occur as conjugated pairs there is indeed a 2π phase accumulation over the real axis.^[51]

As a result, both scenarios leverage on zeros expelled to the upper part of the complex plane to achieve a 2π -phase accumulation caused by the branch cut of one zero-pole pair crossing the real axis. We illustrate both scenarios considering a metasurface composed of square nanocubes with a length $L = 350$ nm and various heights h , made of a dielectric medium with relative permittivity $\epsilon = 8.05$ (which approximately corresponds to Sb_2S_3 phase-change material in the amorphous state) arranged in a 2D

square array with a period $p = 500$ nm. The substrate relative permittivity is equal to $\epsilon_{\text{sub}} = 2.25$ while the relative permittivity of the top medium will be varied in the following examples. The numerical calculations of the optical response of these metasurfaces for complex-valued frequencies are performed using JCMSuite, a software based on the finite-element method.^[52] For details on the numerical simulations, please see the Section SIV, Supporting Information.

4.1. Explicit Parity-Time Symmetry-Breaking for Phase Engineering in Reflection

To illustrate the first method, we start by considering a PT-symmetric version of the Sb_2S_3 metasurface: it is lossless and the superstrate is a dielectric material with the same relative permittivity as that of the substrate: $\epsilon_{\text{sub}} = \epsilon_{\text{sup}} = 2.25$, making the overall system invariant under reflection with respect to its median plane at $z = 0$. For nanocubes of height 160 nm, it can be seen in Figure 2a that a reflection zero exists on the real axis for $\omega \approx 2.15 \times 10^{15}$ rad s^{-1} . The parity symmetry may be broken simply by changing the dielectric permittivity of the top material to $\epsilon_{\text{sup}} = 2.12$, keeping the substrate permittivity unchanged and preserving the time-reversal symmetry. The results for an incident field impinging from the substrate side are shown in Figure 2b. As a consequence of the parity symmetry breaking, the reflection zero moves upward. A drastic change of the behavior of the reflection coefficient phase in the ω -plane can thus be observed. The plot of the phase dependency for real frequencies in Figure 2a shows that there is a phase discontinuity when the zero is located on the real axis. On the other hand, the phase varies from 0 to beyond 2π when the zero moves to the upper part of the complex plane as seen in Figure 2b. The reason why the phase accumulation exceeds 2π is the existence of another zero-pole pair in the lower part of the complex plane for larger frequencies (see Supporting Information). Transposing this to the transmission case, that is moving up the transmissionless states, requires breaking the time-reversal symmetry by adding gain in the metasurface.^[53]

4.2. Spontaneous Symmetry-Breaking at EP for Phase Engineering in Transmission

Let us now illustrate the second approach. The map of the phase of the transmission coefficient of the Sb_2S_3 metasurface for nanocube height equal to 190 nm is displayed in Figure 2c showing the existence of two zeros on the real axis. Decreasing the nanocube height to 160 nm, qualitatively modifies the complex transmission map. The two zeros leave the real axis and form a conjugated pair below and above the real axis, as shown in Figure 2d. This is an example of spontaneous time-reversal symmetry breaking of the states.^[54] The existence of a transmission zero in the upper half of the complex plane provides a full 2π accumulation over the real axis. It is confirmed by looking at the phase accumulation as a function of the real frequency on the left bottom plot in Figure 2d. We emphasize that this approach would work in reflection, where a spontaneous breaking of the P or T -symmetry would result in the appearance of a conjugated pair of reflection zeros as well.

4.3. Coalescence of Zeros at the Exceptional Points: the Topological Origin of the Huygens Metasurfaces

The origin of the spontaneous symmetry breaking observed in Figure 2d requires the interaction between several zero-pole pairs. To study this interaction, the height of the considered metasurface is gradually varied from $h = 120$ nm to $h = 200$ nm. The maps of the amplitude and phase of the metasurface as a function of the height of the metasurface nanocubes and frequency are shown in Figure 3a,b. These maps reveal a behavior identical to the one reported for dielectric Huygens metasurfaces (HMS)^[24] with the existence of a range of heights for which the amplitude of the transmission coefficient becomes large and the phase covers the full 2π interval. The real and imaginary parts of transmission zeros as a function of the height of the metasurface nanocubes are shown in Figure 3b,c. Outside the HMS operating region, the two zeros occur for two different real parts but share the same imaginary part (which vanishes). However, the two zero real parts converge close to the boundaries of the HMS operating region and their real parts become identical at the boundaries of this region. Their imaginary parts split into two values that are symmetric with respect to the real axis. Analyzing the trajectories of the transmission zeros thus allows us to link the operating region of HMS occurring between $h \approx 142$ nm and $h \approx 183$ nm to the range of heights where transmission zeros exist as a conjugated pair in the complex plane, which corresponds to the regime of spontaneously broken time-reversal symmetry and to the existence of two transmission zero degeneracies, also called exceptional points (EPs),^[55] at the boundaries of the HMS operating region. Avoided crossing of two zero-pole pairs moves one of the zeros in the upper part of the complex plane satisfying the sufficient branch cut crossing condition required to achieve 2π phase coverage. The EPs are found for $h_{\text{EP1}} = 183.58$ nm and $h_{\text{EP2}} = 142.88$ nm. EPs are a type of degeneracies specific to non-Hermitian systems.^[56,57] At the degeneracy, not only do the eigenfrequencies become identical but their associated eigenstates coalesce. In the field of metasurfaces, the coalescence of eigenstates at an EP has been used for the design of polarization-dependent metasurfaces recently.^[58] EP have also been proven useful in many other applications,^[59] in particular for sensing.^[60,61] Figure 3d represents the phase of the transmission coefficient in the complex frequency plane around EP1. The circulation of the phase around the zero indicates that it is a second-order zero with phase winding equal to 4π leading to a topological charge equal to $q = +2$, as expected for an EP. To illustrate how the trajectories of zeros are linked to the existence of these two EPs, we fit these trajectories with a superposition of a linear dependency with h and a square root function with two zeros thus featuring two square-root branch points at the positions of the two EPs

$$\omega_{\text{TZ,EP1/EP2}}(h) = a h + b \pm c \sqrt{(h_{\text{EP1}} - h)(h_{\text{EP2}} - h)} \quad (3)$$

the constants a , b , and c are determined by fitting leading to the following values: $a = -2.3465 \times 10^{21}$ $\text{s}^{-1} \text{m}^{-1}$, $b = 2.5317 \times 10^{15}$ s^{-1} , and $c = 8.462 \times 10^{20}$ $\text{s}^{-1} \text{m}^{-1}$. The predictions of this fitting model are shown by red and black lines in Figure 3b,c. A good qualitative agreement between the trajectories of zeros and the fitting function is found for both the real and imaginary parts.

For height smaller than 130 nm, a deviation between the fitting model $\omega_{TZ,-}(h)$ and the position of zeros determined by the numerical calculations (black dots and line) is observed. EPs are, by definition, square-root branch point singularities corresponding to conditions for which the expression under the square-root sign vanishes. This confirms that spontaneous symmetry breaking occurs at exceptional points of transmissionless states. Here only the height of the nanocubes is tuned to obtain these EPs, while these are usually found by tuning two parameters. This is a consequence of the underlying symmetries of the system as pointed out in ref. [62]. An important consequence of the discovery of this mechanism is that it provides a fundamental explanation of the physics underlying the design of widely used dielectric Huygens metasurfaces (HMS).^[24,63–79] The original understanding of HMS properties relied exclusively on a spectral overlap of electric and magnetic dipolar resonances, which was derived following a theoretical modal analysis of arrays of spherical silicon particles.^[80] By carefully studying the trajectories of zeros, we prove that the boundaries of the 2π phase change regions correspond to EPs where two transmission zeros become degenerated. We also computed the electric and magnetic resonance frequencies of this Sb_2S_3 metasurface by solving eigenvalue problems,^[81] and the silicon nanodisk metasurface proposed in ref. [24] (see Supporting Information), and we found that they never fully coincide. Our results thus shed a different light on the behavior of HMS by interpreting it from the relative positions of zeros and poles of the transmission coefficients. On the other hand, the behavior of HMS is usually only explained by relying on the electric and magnetic dipolar responses of dielectric metasurfaces. A connection between these two interpretations will be made in Section 5 by calculating the dipolar electric and magnetic susceptibilities of the metasurface considered herein.

Finally, it is worth mentioning that the symmetry considerations used throughout this article were determined for a field impinging on the metasurface at normal incidence. At non-normal incidence angles, additional spatial symmetries of the metasurface play an important role, in particular in-plane symmetries, explaining the high sensitivity of Huygens metasurfaces response with respect to the incident angle.^[82]

5. Electromagnetic Susceptibility Responses of Topological Surfaces and Influence of Absorption Losses

We started in Section 2 with a single zero-pole pair toy-model, then in Section 4 a numerical calculation for a realistic metasurface with several zero-pole pairs and now, in Section 5, we rely on another description GSTC of the metasurface response to specifically investigate the trajectories of transmission zeros. GSTCs are convenient analytical tools to study the metasurface optical responses. They consist of a zero-thickness sheet supporting electric and magnetic dipole responses expressed in terms of effective surface susceptibilities.^[83] In this way, we will be able to link our previous results obtained using symmetry-based discussions to the electric and magnetic dipole responses of metasurfaces which are widely used as a design tool. The effective metasurface susceptibilities provide simple expressions for the reflection

or transmission T coefficients. For a normally propagating incident wave, they read as^[83]

$$R = \frac{2ik(\chi_e - \chi_m)}{(2 - ik\chi_m)(2 - ik\chi_e)} \quad (4a)$$

$$T = \frac{4 + \chi_m\chi_e k^2}{(2 - ik\chi_m)(2 - ik\chi_e)} \quad (4b)$$

where χ_e and χ_m are the metasurface electric and magnetic isotropic susceptibilities and $k = \omega/c$ with c being the speed of light in the metasurface surrounding medium. It is important to notice that magnetic currents generate odd modes and electric currents generate even modes as seen in Figure 4a. Here, even and odd are related to the parity of the solutions with respect to the median plane of the structure $z = 0$. Because of modal symmetry, previous works on HMS rightfully explained that destructive interference between these modes on one or the other side of the metasurface may lead to the appearance of reflection and transmission zeros, also related to the first and second Kerker conditions.^[24] Here, we particularly focus on transmissionless states with zero optical backscattered signals, and show that the GSTC method provides insights on the trajectories of transmission zeros observed in Figure 3.

The GSTC method yields the expressions provided in Equations (4a) and (4b) for the reflection and transmission coefficients where $\chi_e(\omega)$ and $\chi_m(\omega)$ are the electric and magnetic susceptibilities, represented by the Lorentzian functions

$$\chi_{e/m}(\omega) = \frac{A_{e/m}}{(\omega_{e/m}^2 - \omega^2) - i\gamma_{e/m}\omega} \quad (5)$$

where $A_{e/m}$ is the amplitude, $\omega_{e/m}$ is the resonance frequency, and $\gamma_{e/m}$ is the damping factor. All these quantities are determined by fitting from numerical calculations. Reflection, transmission zeros, as well as resonances, may then be found by solving Equations (4a) and (4b). Poles of R and T occur when either of the two following conditions is fulfilled independently for electric or magnetic resonances: $2 - ik\chi_e = 0$ and $2 - ik\chi_m = 0$. However, Equations (4a) and (4b) indicate that reflection and respectively transmission zeros occur when $\chi_e = \chi_m$ and $4 + \chi_m\chi_e k^2 = 0$. A precise mixed contribution of both electric and magnetic susceptibilities is therefore required to obtain transmission zeros which result from the interferences between field distributions of different symmetries. Substituting Equation (5) into the different conditions is used to obtain the complex frequencies of transmission and reflection zeros. The resulting expressions are provided in Equations (S6) to (S10), Supporting Information for the cases of damped ($\gamma_e \neq 0, \gamma_m \neq 0$) and undamped ($\gamma_e = \gamma_m = 0$) metasurfaces. Figure 4c shows the variation of real parts of the transmission zero frequency, the reflection zero frequency, and poles frequencies as a function of the nanocubes height, h . The plot Figure 4d and Video S1, Supporting Information clearly highlight that the high transmission window, known as Huygens metasurface regime, results from pole inversion through avoided crossing of two zero-pole pairs as the geometrical parameters are varied, creating an “opening” near the real axis for the electric zero-pole pair to pass. From the physical point of view, avoided crossing of the pairs is imposed because the trajectories and velocities

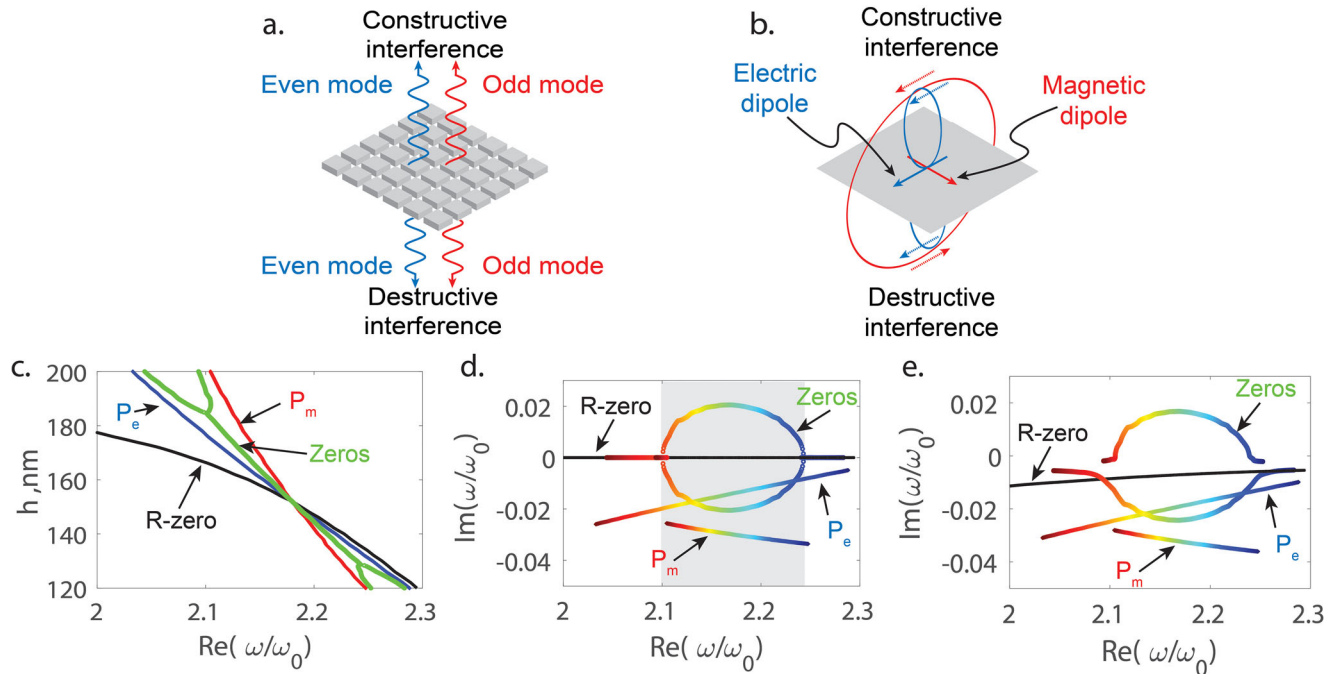


Figure 4. Symmetries of the electric and magnetic modes and avoided crossing in the presence of intrinsic loss. a) Schematic representation of even and odd mode interference at a metasurface presenting unidirectional scattering properties. b) Classical representation of Huygens E and M dipolar interference condition achieving unidirectional scattering in (a). c) Real part of the frequency solutions of GSTCs for transmission zeros, reflection zero (denoted R-zero) and poles (P_e and P_m) positions as a function of the metasurface height. Avoided crossing of pairs occurs at the frequency where all curves intersect around $\text{Re}(\omega) \approx 2.17 \times 10^{15} \text{ rad s}^{-1}$. d) Complex-plane positioning of the reflection zero (R-zero), transmission zeros, and E and M-pole frequencies as a function of the nanocube height (color-coded from blue to red for increasing height). Avoided crossing of the zero–pole pairs occurs such that the “fastest” pole associated with the electric resonances could cross the zero–pole branch cut of the magnetic mode. e) Same as in (d) but in the presence of intrinsic losses, that is, in the regime where explicit symmetry breaking of the time-reversal symmetry is realized. Zeros are expelled from the real axis, but for a similar topological reason as in (d), avoided crossing of the zero–pole branch cut (previously found for time-reversal symmetric system) still occur, this case without degeneracy of zeros at EPs.

of the poles displacements in the complex plane as a function of the height strongly differ due to different modal confinements of the electric and magnetic resonant fields. Poles and zeros are being connected via the branch cut, that is, the line where the phase is discontinuous, and therefore pole inversion in the complex plane cannot occur directly by crossing branch cuts. The only topologically valid solution is to expel the two zeros symmetrically from the real axis, so as to preserve PT-symmetry, in such a way that the “fastest” pole–zero pair in terms of frequency shift as a function of geometrical parameters, could cross, to the other side of the “slow” resonance. Due to larger field confinement, the electric resonance is more sensitive to structural parameter changes and it moves faster with respect to the magnetic mode. Repelling both zeros from the real axis results in a high transmission window while one zero located in the upper part of the complex plane introduces a 2π -phase accumulation that is of interest for metasurface design. Figure 4e shows the same configuration as previously but with additional damping in the GSTC formula ($\gamma_e \neq 0, \gamma_m \neq 0$). In this case, time-reversal symmetry is broken. It can then be noted that there is no EPs of transmission zeros. In fact, it is well known that the tuning of two parameters is usually necessary for reaching an EP. The reason why only one was necessary in the case of the lossless metasurface considered previously was the underlying symmetry of the system,^[62]

in our case time-reversal symmetry. As soon as this symmetry is broken, two parameters are again needed for reaching an EP. In Figure 4e, the zeros thus do not merge, but the avoided crossing behavior remains, leading again to the existence of one zero in the upper half of the complex plane. As a result, the 2π -phase accumulation is still observed without zeros degeneracy and EP, indicating that this approach is robust and would also apply to metasurfaces made of arbitrary materials.

6. Conclusion

In summary, we have proposed a general method to address 2π phase accumulation of the reflected or transmitted light at interfaces. More precisely, a sufficient condition is to have a metasurface presenting a pair of topological phase singularities with opposite charges, the so-called zero–pole pair, located in the complex frequency plane separated by the real axis. In this case, the branch cut connecting them crosses the real axis, thus accumulating a 2π phase as a function of the real frequency. The identification of nanostructure parameters which could lead to this behavior is extremely useful for realizing phase-gradient metasurfaces for optical wavefront control. Relying on symmetry arguments, two simple solutions to achieve such zero–pole separation are provided. The first solution consists of explicitly

breaking the symmetry of the system, either breaking T -symmetry by adding gain or losses or P -symmetry breaking by, for example, disposing the metasurface at the interface between two optically different materials. Symmetry-breaking considerations required for achieving a 2π resonant phase jump not only explain existing metasurface designs, but they might also be deliberately invoked to achieve unexpected and innovative designs. In particular, explicit symmetry-breaking in the z -direction (i.e., perpendicular to the metasurface plane) appears as a new degree of freedom to engineer the phase response of metasurfaces in reflection. The second approach relies on the interaction of two pairs of zeros and poles. In the absence of loss, it was shown that the two zeros can coalesce at an exceptional point of transmissionless states and then bifurcate in the complex plane with one zero then moving in the upper part of the complex plane while the other moves in the lower part of the complex plane. The 2π phase accumulation may survive when loss is added while the EPs vanish. This second approach suggests that topological arguments are at the origin of the physics underlying the design of Huygens metasurfaces. Our discovery on the existence of EP, or second-order topological singularity, in such simple and well-studied Huygens nanostructures could have tremendous applications, in particular, for enhanced-sensing. Besides, harnessing degeneracies of several topological phase singularities and adding other symmetry-breaking conditions would open new design perspectives in nanophotonics. It reveals also that Huygens metasurfaces are a part of a much wider class of metasurfaces (related to branch cut crossing), greatly broadening the range of applicability of this design approach for controlling the phase of light with nanoscale topologically engineered symmetry-breaking structures.

Supporting Information

Supporting Information is available from the Wiley Online Library or from the author.

Acknowledgements

P.G. and N.B. acknowledge financial support by the French National Research Agency ANR Project DILEMMA (ANR-20-CE09-0027). P.G. and E.M. acknowledge financial support by the French National Research Agency ANR Project Meta-On-Demand (ANR-20-CE24-0013). P.G. acknowledges support from the European Innovation Council (EIC) project TwistedNano (under the grant agreement number Pathfinder Open 2021-101046424). P.G. thanks J. Y. Duboz for useful discussions on the part related to complex plane integration. O.M. and K.A. acknowledge funding from the European Research Council (ERC-2015-AdG-695206 Nanofactory) and from the Swiss National Science Foundation (project PZ00P2_193221). R.C. and S.B. acknowledge funding from the German Research Foundation (DFG, Excellence Cluster MATH+, EXC-2046/1, project 390685689) and the Helmholtz Association (Helmholtz Excellence Network SOLARMATH, project ExNet-0042-Phase-2-3).

Open access funding enabled and organized by Projekt DEAL.

Conflict of Interest

The authors declare no conflict of interest.

Data Availability Statement

The data that support the findings of this study are available from the corresponding author upon reasonable request.

Keywords

metasurfaces, nanophotonics, resonant photonics, topological photonics

Received: December 13, 2022

Revised: February 13, 2023

Published online:

- [1] N. Yu, P. Genevet, M. A. Kats, F. Aieta, J.-P. Tetienne, F. Capasso, Z. Gaburro, *Science* **2011**, *334*, 333.
- [2] P. Lalanne, S. Astilean, P. Chavel, E. Cambril, H. Launois, *Opt. Lett.* **1998**, *23*, 1081.
- [3] D. Fattal, J. Li, Z. Peng, M. Fiorentino, R. G. Beausoleil, *Nat. Photonics* **2010**, *4*, 466.
- [4] P. Genevet, N. Yu, F. Aieta, J. Lin, M. A. Kats, R. Blanchard, M. O. Scully, Z. Gaburro, F. Capasso, *Appl. Phys. Lett.* **2012**, *100*, 013101.
- [5] F. Aieta, P. Genevet, N. Yu, M. A. Kats, Z. Gaburro, F. Capasso, *Nano Lett.* **2012**, *12*, 1702.
- [6] A. Pors, M. G. Nielsen, R. L. Eriksen, S. I. Bozhevolnyi, *Nano Lett.* **2013**, *13*, 829.
- [7] E. Karimi, S. A. Schulz, I. De Leon, H. Qassim, J. Upham, R. W. Boyd, *Light: Sci. Appl.* **2014**, *3*, e167.
- [8] Y. Yang, W. Wang, P. Moitra, I. I. Kravchenko, D. P. Briggs, J. Valentine, *Nano Lett.* **2014**, *14*, 1394.
- [9] S. Wang, P. C. Wu, V.-C. Su, Y.-C. Lai, M.-K. Chen, H. Y. Kuo, B. H. Chen, Y. H. Chen, T.-T. Huang, J.-H. Wang, R.-M. Lin, C.-H. Kuan, T. Li, Z. Wang, S. Zhu, D. P. Tsai, *Nat. Nanotechnol.* **2018**, *13*, 227.
- [10] W. T. Chen, A. Y. Zhu, V. Sanjeev, M. Khorasaninejad, Z. Shi, E. Lee, F. Capasso, *Nat. Nanotechnol.* **2018**, *13*, 220.
- [11] H. Ren, G. Briere, X. Fang, P. Ni, R. Sawant, S. Héron, S. Chenot, S. Vézian, B. Damilano, V. Brändli, S. A. Maier, P. Genevet, *Nat. Commun.* **2019**, *10*, 2986.
- [12] Q. Song, A. Baroni, R. Sawant, P. Ni, V. Brandli, S. Chenot, S. Vézian, B. Damilano, P. de Mierry, S. Khadir, P. Ferrand, P. Genevet, *Nat. Commun.* **2020**, *11*, 2651.
- [13] R. Sawant, D. Andrén, R. J. Martins, S. Khadir, R. Verre, M. Käll, P. Genevet, *Optica* **2021**, *8*, 1405.
- [14] Q. Song, A. Baroni, P. C. Wu, S. Chenot, V. Brandli, S. Vézian, B. Damilano, P. de Mierry, S. Khadir, P. Ferrand, P. Genevet, *Nat. Commun.* **2021**, *12*, 3631.
- [15] Q. Song, S. Khadir, S. Vézian, B. Damilano, P. D. Mierry, S. Chenot, V. Brandli, P. Genevet, *Sci. Adv.* **2021**, *7*, eabe1112.
- [16] H.-T. Chen, A. J. Taylor, N. Yu, *Rep. Prog. Phys.* **2016**, *79*, 076401.
- [17] P. Genevet, F. Capasso, F. Aieta, M. Khorasaninejad, R. Devlin, *Optica* **2017**, *4*, 139.
- [18] S. M. Kamali, E. Arbabi, A. Arbabi, A. Faraon, *Nanophotonics* **2018**, *7*, 1041.
- [19] W. T. Chen, A. Y. Zhu, F. Capasso, *Nat. Rev. Mater.* **2020**, *5*, 604.
- [20] M. Berry, *J. Mod. Opt.* **1987**, *34*, 1401.
- [21] G. Biener, A. Niv, V. Kleiner, E. Hasman, *Opt. Lett.* **2002**, *27*, 1875.
- [22] V. Grigoriev, A. Tahri, S. Varault, B. Rolly, B. Stout, J. Wenger, N. Bonod, *Phys. Rev. A* **2013**, *88*, 011803.
- [23] V. Grigoriev, S. Varault, G. Boudarham, B. Stout, J. Wenger, N. Bonod, *Phys. Rev. A* **2013**, *88*, 063805.
- [24] M. Decker, I. Staude, M. Falkner, J. Dominguez, D. N. Neshev, I. Brener, T. Pertsch, Y. S. Kivshar, *Adv. Opt. Mater.* **2015**, *3*, 813.
- [25] W. R. Sweeney, C. W. Hsu, A. D. Stone, *Phys. Rev. A* **2020**, *102*, 063511.
- [26] Y. Kang, A. Z. Genack, *Phys. Rev. B* **2021**, *103*, L100201.
- [27] While the results presented here can be extended to multiport cases, we consider for simplicity and throughout the rest of this paper only one input and one output modes. Regarding symmetry considerations discussed further, we fix the input incident angle at

- normal incidence and consider only the case of polarization preserving metasurfaces.
- [28] L. C. Botten, M. Cadilhac, G. Derrick, D. Maystre, R. McPhedran, M. Nevière, P. Vincent, *Electromagnetic Theory of Gratings*, Vol. 22, Springer Science & Business Media, Berlin 2013.
- [29] M. Hutley, D. Maystre, *Opt. Commun.* **1976**, 19, 431.
- [30] D. Maystre, in *Plasmonics*, Springer, Berlin 2012, pp. 39–83.
- [31] D. Maystre, *C. R. Phys.* **2013**, 4, 381.
- [32] G. J. Gbur, *Singular Optics*, CRC Press, Boca Raton, FL 2016.
- [33] J. F. Nye, *Natural Focusing and Fine Structure of Light: Caustics and Wave Dislocations*, CRC Press, Boca Raton, FL 1999.
- [34] M. Soskin, M. Vasnetsov, *Prog. Opt.* **2001**, 42, 219.
- [35] M. R. Dennis, K. O'holleran, M. J. Padgett, *Prog. Opt.* **2009**, 53, 293.
- [36] H. M. Nussenzveig, *Causality and Dispersion Relations*, Academic Press, Cambridge, MA 1972.
- [37] N. Van Kampen, *Phys. Rev.* **1953**, 89, 1072.
- [38] J. S. Toll, *Phys. Rev.* **1956**, 104, 1760.
- [39] G. B. Arfken, H. J. Weber, *Mathematical Methods for Physicists*, Academic Press, Cambridge, MA 1999.
- [40] N. D. Mermin, *Rev. Mod. Phys.* **1979**, 51, 591.
- [41] Y. Chong, L. Ge, H. Cao, A. D. Stone, *Phys. Rev. Lett.* **2010**, 105, 053901.
- [42] Poles of S -matrix are complex solutions of wave equation calculated with only outgoing boundary conditions, while zeros of S are calculated with only in-going boundary conditions. Poles and zeros of S -matrix are not independent: in the lossless system, they are always complex conjugates due to the time-reversal symmetry.^[41] It is also not possible to bring poles and zeros to the real frequency axis without gain-loss engineering due to energy conservation.^[23]
- [43] Reflectionless scattering modes (RSM)^[25] and transmissionless scattering modes (TSM)^[26] are often used in the literature to denote the two specific cases when zeros are brought to the real axis, which could occur even in lossless systems. The rest of the time, that is for any value of the zero-frequency in the complex plane, the states are called reflectionless and respectively transmissionless states.
- [44] H. Shen, B. Zhen, L. Fu, *Phys. Rev. Lett.* **2018**, 120, 146402.
- [45] R. A. Depine, V. L. Brudny, J. M. Simon, *Opt. Lett.* **1987**, 12, 143.
- [46] A. Pors, S. I. Bozhevolnyi, *Opt. Express* **2013**, 21, 27438.
- [47] A. Berkhout, A. F. Koenderink, *ACS Photonics* **2019**, 6, 2917.
- [48] D. B. Haim, L. Michaeli, O. Avayu, T. Ellenbogen, *Opt. Express* **2020**, 28, 17923.
- [49] Y.-W. Huang, H. W. H. Lee, R. Sokhoyan, R. A. Pala, K. Thyagarajan, S. Han, D. P. Tsai, H. A. Atwater, *Nano Lett.* **2016**, 16, 5319.
- [50] C. Qu, S. Ma, J. Hao, M. Qiu, X. Li, S. Xiao, Z. Miao, N. Dai, Q. He, S. Sun, L. Zhou, *Phys. Rev. Lett.* **2015**, 115, 235503.
- [51] While it is usual to look at the trajectories of resonance eigenfrequencies alone (crossing and anti-crossing), these results indicate that understanding of similar avoided crossing mechanisms in non-Hermitian systems requires to study the trajectories of the zero-pole pairs as a whole.
- [52] J. Pomplun, S. Burger, L. Zschiedrich, F. Schmidt, *Phys. Status Solidi B* **2007**, 244, 3419.
- [53] Note that to observe the resonant 2π phase accumulation, pole and zero still have to be positioned across the real axis. It means that the amount of added gain has to be carefully chosen for the pole to remain alone in the lower part of the complex plane. Note however that when the gain is added and poles are getting closer and closer to the real axis, nonlinear effects may become important. The description of a pole and zero positioning in the nonlinear regime is out of the scope of the present studies.
- [54] Y.-K. Lu, P. Peng, Q.-T. Cao, D. Xu, J. Wiersig, Q. Gong, Y.-F. Xiao, *Sci. Bull.* **2018**, 63, 1096.
- [55] W. R. Sweeney, C. W. Hsu, S. Rotter, A. D. Stone, *Phys. Rev. Lett.* **2019**, 122, 093901.
- [56] W. Heiss, *J. Phys. A: Math. Theor.* **2012**, 45, 444016.
- [57] B. Zhen, C. W. Hsu, Y. Igarashi, L. Lu, I. Kaminer, A. Pick, S.-L. Chua, J. D. Joannopoulos, M. Soljačić, *Nature* **2015**, 525, 354.
- [58] Q. Song, M. Odeh, J. Zúñiga-Pérez, B. Kanté, P. Genevet, *Science* **2021**, 373, 1133.
- [59] M.-A. Miri, A. Alu, *Science* **2019**, 363, eaar7709.
- [60] J. Wiersig, *Phys. Rev. Lett.* **2014**, 112, 203901.
- [61] J.-H. Park, A. Ndao, W. Cai, L. Hsu, A. Kodigala, T. Lepetit, Y.-H. Lo, B. Kanté, *Nat. Phys.* **2020**, 16, 462.
- [62] M. Fruchart, R. Hanai, P. B. Littlewood, V. Vitelli, *Nature* **2021**, 592, 363.
- [63] J. Cheng, D. Ansari-Oghol-Beig, H. Mosallaei, *Opt. Lett.* **2014**, 39, 6285.
- [64] Y. F. Yu, A. Y. Zhu, R. Paniagua-Domínguez, Y. H. Fu, B. Luk'yanchuk, A. I. Kuznetsov, *Laser Photonics Rev.* **2015**, 9, 412.
- [65] L. Wang, S. Kruk, H. Tang, T. Li, I. Kravchenko, D. N. Neshev, Y. S. Kivshar, *Optica* **2016**, 3, 1504.
- [66] Q.-T. Li, F. Dong, B. Wang, F. Gan, J. Chen, Z. Song, L. Xu, W. Chu, Y.-F. Xiao, Q. Gong, Y. Li, *Opt. Express* **2016**, 24, 16309.
- [67] W. Zhao, H. Jiang, B. Liu, J. Song, Y. Jiang, C. Tang, J. Li, *Sci. Rep.* **2016**, 6, 30613.
- [68] M. M. Shanei, M. Hashemi, D. Fathi, C. J. Zapata-Rodríguez, *Appl. Opt.* **2017**, 56, 8917.
- [69] Z. Zhou, J. Li, R. Su, B. Yao, H. Fang, K. Li, L. Zhou, J. Liu, D. Stellinga, C. P. Reardon, T. F. Krauss, X. Wang, *ACS Photonics* **2017**, 4, 544.
- [70] J. Bar-David, N. Mazurski, U. Levy, *ACS Photonics* **2017**, 4, 2359.
- [71] J. Tian, Y. Yang, M. Qiu, F. Laurell, V. Pasiskevicius, H. Jang, *Opt. Express* **2017**, 25, 24068.
- [72] S. Liu, A. Vaskin, S. Campione, O. Wolf, J. L. Reno, G. A. Keeler, I. Staude, I. Brener, *Nano Lett.* **2017**, 17, 4297.
- [73] A. J. Ollanik, J. A. Smith, M. J. Belue, M. D. Escarra, *ACS Photonics* **2018**, 5, 1351.
- [74] G. Yoon, D. Lee, K. T. Nam, J. Rho, *ACS Photonics* **2018**, 5, 1643.
- [75] P. P. Iyer, N. A. Butakov, J. A. Schuller, *ACS Photonics* **2015**, 2, 1077.
- [76] A. Komar, Z. Fang, J. Bohn, J. Sautter, M. Decker, A. Miroshnichenko, T. Pertsch, I. Brener, Y. S. Kivshar, I. Staude, D. N. Neshev, *Appl. Phys. Lett.* **2017**, 110, 071109.
- [77] S.-Q. Li, X. Xu, R. Maruthiyodan Veetil, V. Valuckas, R. Paniagua-Domínguez, A. I. Kuznetsov, *Science* **2019**, 364, 1087.
- [78] A. Leitis, A. Hefßler, S. Wahl, M. Wuttig, T. Taubner, A. Tittl, H. Altug, *Adv. Funct. Mater.* **2020**, 30, 1910259.
- [79] I. Staude, A. E. Miroshnichenko, M. Decker, N. T. Fofang, S. Liu, E. Gonzales, J. Dominguez, T. S. Luk, D. N. Neshev, I. Brener, Y. Kivshar, *ACS Nano* **2013**, 7, 7824.
- [80] A. B. Evlyukhin, C. Reinhardt, A. Seidel, B. S. Luk'yanchuk, B. N. Chichkov, *Phys. Rev. B* **2010**, 82, 045404.
- [81] F. Binkowski, L. Zschiedrich, S. Burger, *J. Eur. Opt. Soc. Rapid Publ.* **2019**, 15, 3.
- [82] C. Gigli, Q. Li, P. Chavel, G. Leo, M. L. Brongersma, P. Lalanne, *Laser Photonics Rev.* **2021**, 15, 2000448.
- [83] K. Achouri, C. Caloz, *Electromagnetic Metasurfaces: Theory and Applications*, Wiley-IEEE Press, Piscataway, NJ 2021.